Capacitively-coupled dual ring antennas for bolt loosening detection

Kang Jiang [a], Liyu Xie [a], Songtao Xue [a,b,*], Guochun Wan [c]

[a] *Department of Disaster Mitigation for Structures, Tongji University, Shanghai, China*
[b] *Department of Architecture, Tohoku Institute of Technology, Sendai, Japan*
[c] *Department of Electronic Science and Technology, Tongji University, Shanghai, China*

ARTICLE INFO

ABSTRACT

This paper proposes a passive and wireless UHF (Ultra High Frequency, operating in 450–550 MHz) antenna sensor for bolt loosening detection. The novelty of this sensor is the introduction of nut's rotation angle as sensing variable, achieving the whole process of bolt status monitoring, and easy installation enabling the sensor to be applied in in-service bolt loosening monitoring. The sensor consists of two concentric rings, and the overall size is 116 mm × 92 mm × 2.4 mm. When the bolt is loose, the nut's rotation will change the coupling capacitance of the antenna and thus the resonant frequency. The electromagnetic performance of the sensor is simulated in HFSS and the quality factor calculated by HFSS is 52.87. Furthermore, the ability to characterize bolt's status was validated in the experiments. The results demonstrate that the resonant frequency increases linearly with the loosening of the bolt (the correlation coefficient is 0.9789) and the antenna's sensitivity is 2.95 MHz/degree.

1. Introduction

Bolted joints have always been considered essential due to their beneficial aspects, such as high installation accuracy, low cost, commercial availability, and variable connection directions, making them the most common connection type in construction [1–3]. The preload of a bolt can provide sufficient connection strength for most supporting construction member. However, during the service life of the structures, many harmful conditions occur; thus, significant impact, dynamic loads, and fatigue loads can inevitably lead to preload degradation of bolted joints, causing local stiffness degeneration and a weakened structural bearing capacity of the structure. Such events can eventually cause destruction of an entire structure [4].

Hence, it is essential to implement precise and high-efficiency technology to monitor the state of bolt loosening and prevent structural collapse. The loosening of bolts is generally recognized to be a time-dependent process, with the preload decreasing as time passes [5]. Typically, the loosening of bolts can be divided into two stages: (1) early stage loosening caused by material deformation [6] and (2) later stage loosening with apparent rotation between the nut and bolt shaft. Several conventional detection methods have evaluated bolt early-stage looseness, including torque detection methods and percussion approaches.

The torque detection method is straightforward where the inspectors check the torque of the bolt directly with a torque wrench to determine whether a bolt is loose. Still, this method requires manually inspecting bolts one by one. The percussion approach requires skilled workers to judge the status of a bolt based on its tapping sound [7]. However, this approach is not appropriate in all circumstances. For example, bolted connections located in extreme conditions often lack proper inspections due to worker difficulty working in extremely cold, icy, or windy conditions. Large-scale bolt looseness detection requires a substantial quantity of effort and time, and the costs of repair are not always easy for proprietors to obtain. Vision inspection is another typical detection method that focuses on the second stage of bolt loosening, which relies on digital images or videos capturing the rotation between the nut and bolt shaft to assess bolt looseness [8,9]; however, current vision inspection monitoring has limited accuracy.

In addition, several novel structural health monitoring (SHM) technologies have developed rapidly to detect bolt looseness, which can be roughly separated into the following categories: the ultrasonic-based method [10], the vibration-based method [11], and the impedance-based method [12]. The ultrasonic-based method can identify the preload status of the bolt by analyzing the ultrasonic waves' time-of-flight (TOF) in the bolts, the ultrasonic velocity ratio between longitudinal and

---

shear waves, and the shift of mechanical resonance frequency. However, the ultrasonic-based measurement is susceptible to environmental interference, which limits its application. The principle of the vibration-based method is based on recording and analyzing dynamic responses to evaluate bolt status when the structure is exposed to vibration loads [11]. However, since vibration responses are primarily dependent on inputs, the vibration-based technique is more suited to identifying global damage. The impedance-based method was created to establish a connection between impedance variations and bolt looseness; however, it can be severely affected by environmental factors, especially temperature, and the measurement equipment is expensive [13].

Recently, various emerging smart materials have been proposed to detect bolt looseness [14]. Huo et al. proposed a piezoceramic transducer that embeds two smart washers into the bolt, each consisting of a piezoceramic patch and flat metal rings [15]. The bolt preload loss can be calculated by analyzing the stress wave generated by the smart washer. Fiber optic sensors are also utilized to measure bolt looseness. The optical fiber is wrapped around the washer to detect the circumferential strain that has a linear relationship with the preload [16]. Although these methods have shown an attractive potential for detecting bolt looseness, their drawbacks are also apparent. These include the need for cables, complicated systems, inconvenient installation, and a continuous power supply, making them unsuitable for long-term and real-time monitoring.

Fortunately, radio-frequency-identification (RFID), a communication technology with salient features such as passive and wireless, provides technical support for building low-cost, passive and large-scale wireless sensor networks. In the RFID technology, antenna sensors develop rapidly due to due to their low-cost, small size, easy installation and simple structure [17].The basic principle is that the input impedance and radar cross section (RCS) of the antenna tag are clearly related to the physical and geometric characteristics of the real target [18]. According to the way of signal sensing, antenna sensors can be classified into two categories: magnetic resonant coupling sensors which operate in low frequency (LF) or high frequency (HF) bands and electromagnetic (EM) coupling (propagation mode) sensors which operate in ultra-high frequency (UHF) and ultra-wide band (UWF) [19]. Alamin et al. [20] used the principle of inductive coupling to monitor the time-domain response of LF RFID tags to detect corrosion, but the read range is limited to 3 cm. Compared with magnetic resonant coupling sensors, electromagnetic coupling sensors have a longer communication distance. Khalifeh et al. [21] utilized corrosion-sensitive microstrip resonators integrated into antenna sensors for corrosion monitoring, and the read range can reach 2 m. The increase of read rang expands the application scenarios of antenna sensors.

Up to now, antenna sensors have been widely used in deformation monitoring [22–24], corrosion monitoring [21,25], temperature monitoring [26,27], moisture monitoring [28,29] and gas monitoring [30,31]. Marindra et al. [32]developed a multi-resonance chipless RFID sensor tag for crack and corrosion monitoring, using principal component analysis(PCA)-based feature extraction and selection to characterize metal crack with different widths and orientations. Borgese et al. [33]presented a humidity sensor based on an Artificial Impedance Surface(AIS) chipless tag, encoding the relative humidity information in the frequency shift, which has a high sensitivity on the small variation of the RH level. Wu et al. [34] proposed an ammonia sensor which load sensitive material onto the antenna. The resistance of the sensitive material will change with ammonia injection, thus shifting the antenna resonant frequency. Xu et al. [35] proposed a strain sensor based on a microstrip patch antenna, and the experiment of wireless interrogation was carried out on the sensor. Mohammad et al. [36] developed a rectangular patch antenna for crack detection based on the principle that conductivity can change with the crack growth in the ground plane, causing a shift in the resonant frequency of the antenna sensor. Yao et al. [37] proposed a temperature sensor that establishes a temperature-frequency relationship by utilizing the properties of dielectric constant

and temperature. However, the aforementioned sensors are all based on a monolithic patch antenna that faces issues such as an incomplete strain transfer ratio and insufficient bonding strength, limiting the accuracy of measurement when used to monitor deformation information [38]. An alternative solution to this issue is to make the antenna sensor unstressed. Xue [38] proposed a crack sensor based on staked rectangular patch antenna. The increase in crack width leads to the change of antenna overlap length, causing the resonant frequency to shift. Caizzone et al. [39] proposed another form of crack sensor based on two planar-inverted-F antennas which employ the phase as the sensing parameter. Zhang et al. [40] proposed a circular antenna sensor for surface crack monitoring. The sensing principle is based on that the increase of crack depth will cause the increase of the effective electrical length of the current flow on the metallic surface. Unstressed antenna sensors have undergone research in various fields of structural health monitoring [41,42], which have shown that the unstressed antenna sensor is more suitable than the monolithic antenna sensor for civil engineering monitoring.

Recently, Xue [43] applied an unstressed patch antenna sensor to monitor bolt looseness by measuring the longitudinal elongation of the whole bolt shaft. However, in practice, holes must be drilled through the bolt shaft to monitor the longitudinal extension of bolts. Hence this technology is incompatible with current in-service bolts. Wu et al. [44] used the reception of RFID sensor signals as a criterion for determining bolt looseness. In the initial state, the RFID tag is covered by a metal film and the reader cannot receive the radio-frequency signal. When the bolt is loose, the tag is exposed outside the metal film, and the reader receives a signal to determine bolt looseness. However, this sensor can only judge whether the bolt is completely loose or not, and cannot monitor the bolt state in real time, and cannot play the role of loosening warning. Matsunaga et al. [45] proposed a waveguide-based sensor to detect bolt looseness. The state of the bolt affects the resistance of the transmission line, thus changing the sensor's effective length and resonance frequency. But the clear frequency response of the sensor can only be observed if the rotation angle of nut exceeds 12 degrees. Currently, wireless sensors used in bolt loosening monitoring have some limitations, such as the inability to monitor the real-time condition of bolt preload, and the sensor's placement necessitates the use of supporting bolts. Therefore, a new type of wireless sensor is urgently required to address these issues.

This paper proposes a novel passive monitoring method for bolt loosening detection based on capacitive-coupled unstressed dual ring antennas. This approach, like the vision-based detection method, does not monitor the axial force of the bolt but rather the rotation angle between the fasteners and connection parts, which determines the loosening status of the bolt. Therefore, there is no need to change the bolts, and the loosening of structural in-service bolts can be tracked. Furthermore, in this method, the looseness status of bolts can be identified by interrogating the proposed sensor wirelessly, overcoming the drawback of visual-based methods that cannot provide round-the-clock, coverage-defying detection and providing higher resolution than the majority of visual-based methods (2.74 degrees) [46]. The proposed sensor comprises two concentric ring antennas attached to the nut and the connection parts, respectively. The inner and outer rings allow current to flow via two stubs, generating the coupling capacitance within the antenna. Through proper installation, the rotation of the nut will rotate the inner ring, changing the coupling capacitance inside the antenna and consequently causing the resonance frequency of the antenna to shift. In this detection method, the dual ring antennas act as a sensing unit and a communication unit simultaneously, and the resonant frequency of the sensor serves as a characterization of the bolt's loosening status.

The rest of the paper is organized as follows: Section 2 introduces the design principle and sensing theory of the sensor; In Section 3, a finite element simulation of the sensor is carried out in a high frequency structure simulator (HFSS). In Section 4, the sensor is made and related
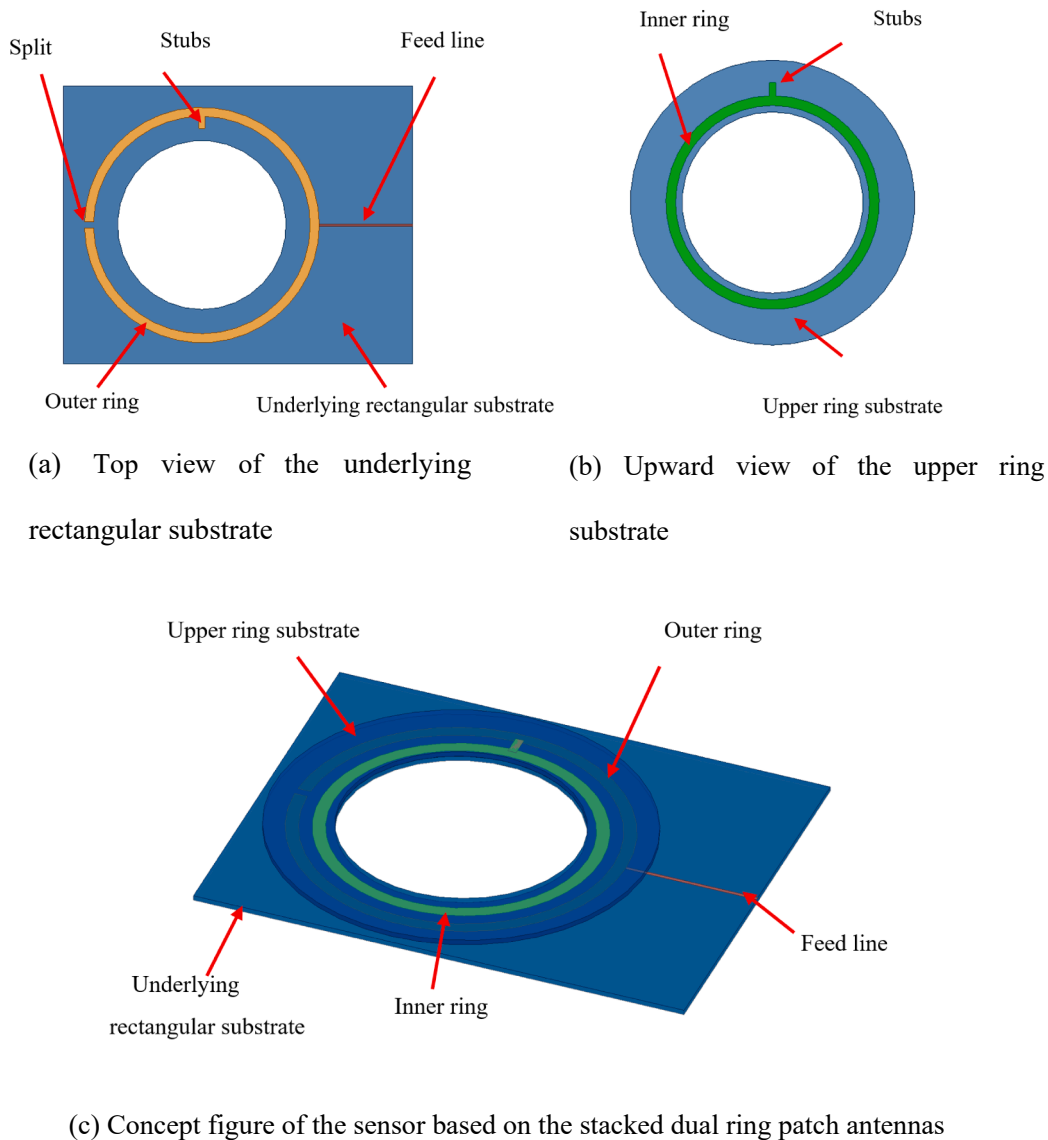
(a) Top view of the underlying rectangular substrate

(b) Upward view of the upper ring substrate

(c) Concept figure of the sensor based on the stacked dual ring patch antennas

Fig. 1. The stacked dual ring patch antennas.

experiments are carried out in the laboratory.

2. Methodology

In this section, an innovative passive method for bolt loosening detection is demonstrated. Unlike the direct monitoring approaches, which are carried out by estimating the bolt preload, this approach takes secondary parameters (the rotation angle of the nut) as characteristics of bolt looseness. An antenna sensor is employed to detect the angle shift between the nut and the gasket caused by bolt looseness in this method. The frequency information of the antenna sensor can be received when the sensor is queried wirelessly by electromagnetic waves, enabling the nut's rotation angle to be restored and the status of the bolt preload to be determined. The relevant design and principles of the sensor are described as follows.

2.1. Design

The proposed sensor is based on stacked dual-ring patch antennas for bolt loosening detection as shown in Fig. 1. The stacked dual-ring patch antennas are formed by an outer split ring antenna and an inner ring

antenna. The outer split ring is etched on the top surface of the underlying rectangular substrate, as shown in Fig. 1(a) and is mounted on the connection part; the inner ring is etched on the bottom surface of the upper ring substrate, as shown in Fig. 1(b) and is fixed with the nut. Due to the tight-fitting design of the upper and underlying substrates, the inner and outer rings should be in the same plane and together constitute the radiation unit, as shown in Fig. 1(c). The inner and outer rings have the same thickness, and circular holes of the same size are cut in the center of the upper and underlying substrate, allowing the sensor to be nested on the outside edge of the bolt. Specifically, a split in the outer ring antenna cuts off the flow of current across the whole outer ring. Meanwhile, the inner ring has an outward stub short-circuited to the outer ring, and the outer ring has an inward stub short-circuited to the inner ring. This short-circuited configuration in the dual ring antennas realizes the current flow through the inner and outer rings, generating coupling capacitance between the inner ring and outer ring.

In actual applications, the underlying rectangular substrate is directly mounted to the connection part, as shown in Fig. 2(a), and the center hole design allows the bolt to be nested in the underlying rectangular substrate. The upper ring substrate is securely connected with the nut through a transparent plate, as shown in Fig. 2(b), and the
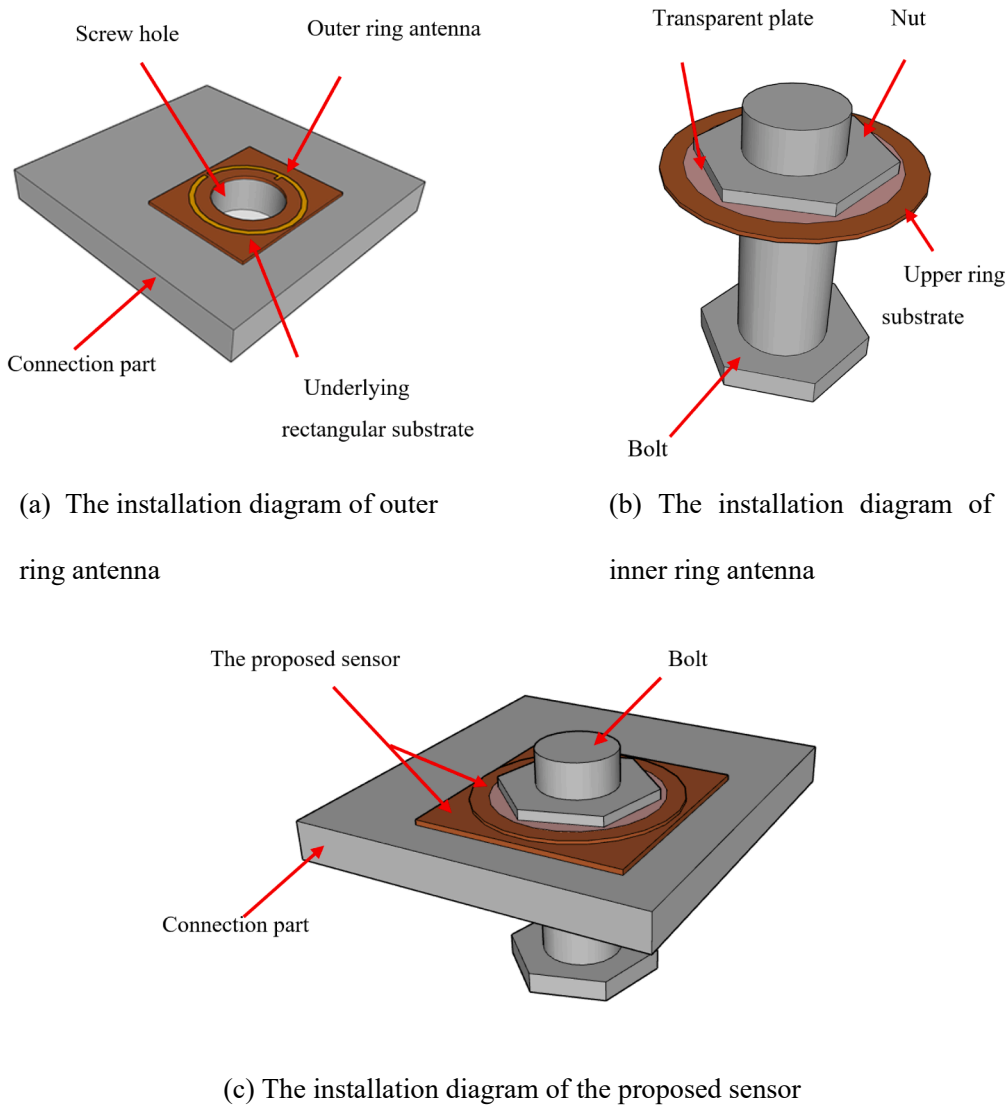
(a) The installation diagram of outer ring antenna

(b) The installation diagram of inner ring antenna

(c) The installation diagram of the proposed sensor

Fig. 2. A detailed installation diagram of the proposed sensor.

rotation of the nut and the rotation of the upper ring substrate can be synchronized. The upper and underlying substrates must be fastened together such that the inner and outer rings are in the same plane, as shown in Fig. 2(c). A short circuit is formed between the inner ring and outer ring by integrating the two stubs. When the bolt preload is degraded, the nut rotates on the screw, causing the upper substrate to rotate relative to the underlying substrate. In this case, the inner ring antenna rotates relative to the outer ring antenna, tuning the coupling capacitance within the dual ring antenna and hence changing the dual ring antenna's resonance frequency. Then the rotation angle of the nut can be restored by post-processing the resonant frequency data of the dual ring antennas, which can be utilized to identify the preload status of bolts.

2.2. Theory of the staked dual ring antennas

The dual ring patch antennas are fed by a feedline connected to the outer ring antenna. Once the antenna is activated, surface currents are first generated on the outer ring. Then, the surface current flows from the outer ring to the inner ring through the stubs, consequently generating a coupling capacitance between the inner and outer rings and a coupling capacitance between the two stubs. The top view of the proposed stacked dual ring patch antennas (the upper substrate is hidden to
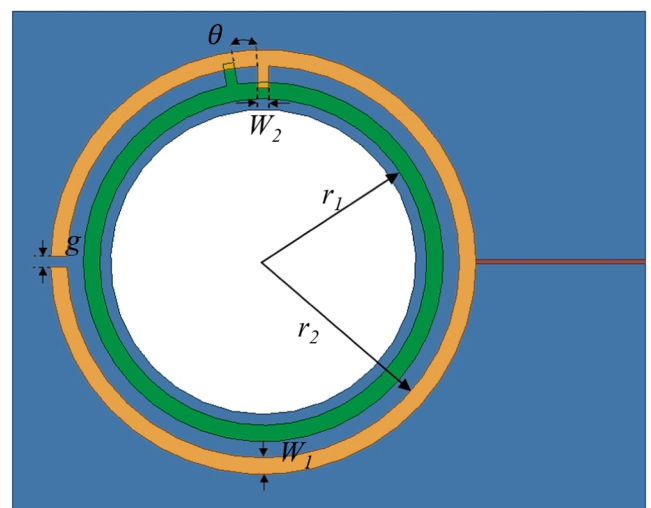

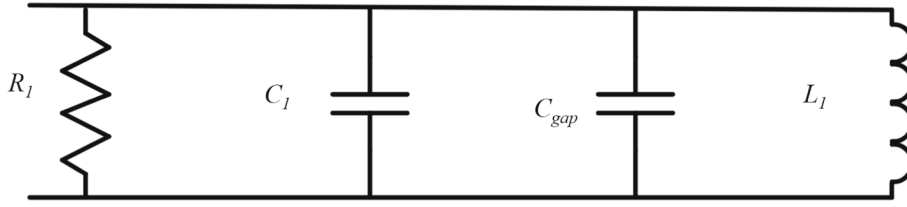**Fig. 3.** A top view of the stacked dual ring patch antennas.

Fig. 4. Equivalent circuit of the dual ring patch antennas in the fundamental resonance mode.

demonstrate the details of the sensor clearly) as shown in Fig. 3.

According to the current distribution of the dual ring antennas, the resonant behavior of dual ring antennas can be divided into two modes: the single resonance mode of the outer ring (the fundamental resonance mode) and the coupling resonant mode of the inner and outer rings (the high-order resonance mode).

In the single resonance mode, the distribution of the surface current is concentrated on the outer ring, and no coupling effect exists between the inner and outer rings owing to the lack of surface current in the inner ring. Thus, only the outer ring serves as the radiation element and can be represented by a parallel lumped LC circuit [47], as shown in Fig. 4. R_1 and L_1 are the equivalent impedance and equivalent inductance of the outer ring antenna, respectively. C_1 is the surface capacitance of the outer ring antenna generated by the charges on the outer ring's surface, and C_{gap} is the split capacitance. Assuming the dielectric constant of the lower substrate is equal to the dielectric constant of the upper substrate, these parameters can be calculated as [48–50]:

$$L_1 = \mu \left(r_2 + \frac{W_1}{2} \right) \left(\ln \frac{8r_2}{h_1 + W_1} \right) \tag{1}$$

$$C_1 = \frac{20\varepsilon(h_1 + W_1)}{\pi} \ln \frac{4r_2}{g} \tag{2}$$

$$C_{gap} = \frac{\varepsilon h_1 W_1}{g} + \varepsilon(h_1 + W_1 + g) \tag{3}$$

where μ is the permeability of the dielectric substrate; r_2 is the radius of the outer ring; ε is the dielectric constant of the dielectric substrate, and W_1 is the thickness of the outer ring and the inner ring. h_1 is the height of the patch antenna, which can be ignored, and g is the gap width.

Due to the short circuit between the inner and outer ring, the surface current of the outer ring flows only three-quarters of the way around the outer ring and flows to the inner ring at the stubs. Therefore, the equivalent inductance of the actual radiation element is only three-fourths of the equivalent inductance of the outer ring, and the equivalent capacitance is only three fourths of the surface capacitance of the outer ring where the split capacitance is ignored. The actual inductance and capacitance are given as:

$$C_{act} = \frac{3}{4}C_1 \tag{4}$$

$$L_{act} = \frac{3}{4}L_1 \tag{5}$$

where C_{act} is the actual capacitance of the radiation element, and L_{act} is the actual inductance of the radiation element.

Then, the fundamental resonant frequency of the dual ring patch antenna can be calculated as:

$$f_1 = \frac{1}{2\pi\sqrt{L_{act}C_{act}}} \tag{6}$$

Obviously, the dimension parameters of the outer ring remain unchanged during the working process of the sensor, so the fundamental resonant frequency of the antenna will be constant.

In the coupling resonant mode of the dual ring antennas, the resonance behavior of the inner ring and outer ring is equivalent to an LC circuit respectively; the electromagnetic coupling effect between two rings can be equivalent to a mutual inductor [24] and a coupling capacitor [51]; the two stubs can be equivalent to the coupling capacitance due to the concentrated distribution of surface current, as shown in Fig. 5. R_1, C_1, C_{gap}, and L_1 have the same meaning as in Fig. 4. R_2, C_2, and L_2 represent the equivalent impedance, surface capacitance and equivalent inductance of the inner ring antenna, respectively. C_{stub} models the coupling capacitance between the stubs, and C_c models the coupling capacitance between the inner ring and the outer ring. M models the mutual inductance between the inner ring and the outer ring.

For the inner ring, the values of the equivalent inductance, L_2, and the surface capacitance, C_2, can be written as [52,53]:

$$L_2 = \frac{\mu h_2 \left\{ J_n(k_1 c) Y_n'(k_1 r_1) - J_n'(k_1 r_1) Y_n(k_1 c) \right\}^2}{\pi k_1^2 N} \tag{7}$$

$$C_2 = \frac{\mu\varepsilon}{L_2 k_1^2} \tag{8}$$

where $N = \frac{1}{2k_1^2} \left[\left(k_1^2 r_2^2 - 1 \right) \left\{ J_n(k_1 r_2) Y_n'(k_1 r_1) - J_n'(k_1 r_1) Y_n(k_1 r_2) \right\}^2 - \frac{4(k_1^2 r_1^2 - 1)}{\pi^2 k_1^2 r_1} \right]$; thus, h_2 is the height of the dielectric substrate; r_1 is the radius of the inner ring; μ is the permeability of the dielectric substrate. J_n' and Y_n' are the first derivatives of Bessel functions of the first and second kind, respectively; c is the distance between the feed point and the center of the inner ring; thus, $c = r_2 + W_1$, while k_1 is the resonant wave number.

Then, the coupled capacitance can be calculated as [54]:

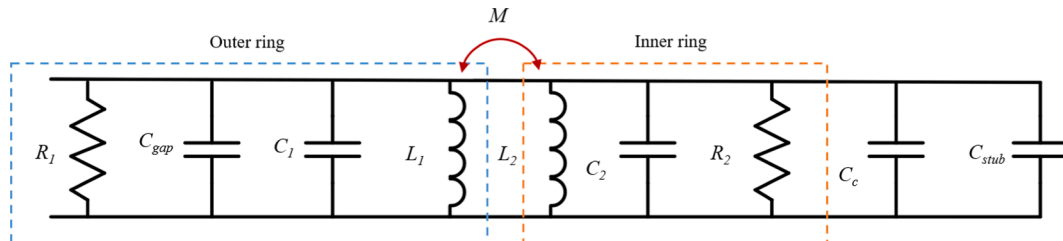$$C_c = \frac{2\pi\varepsilon h_2}{\ln r_2/r_1} \tag{9}$$

Fig. 5. Equivalent circuit of the dual ring patch antennas in the high-order resonance mode.
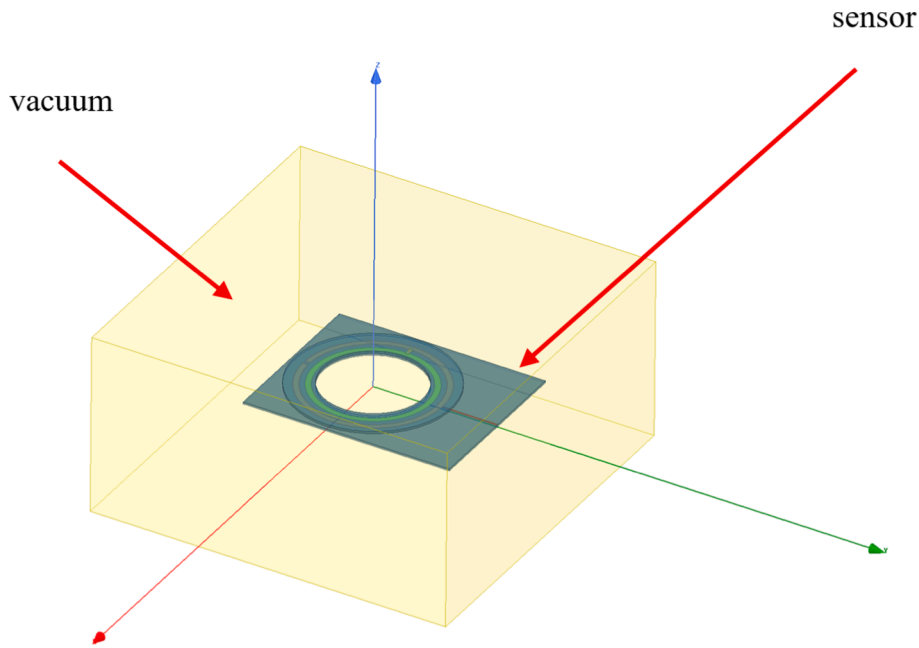
Fig. 6. The finite element model of the sensor in HFSS.

$$C_{stub} = \frac{\varepsilon(r_2 - r_1 - W_1)}{\theta}\ln r_2/r_1 \qquad (10)$$

where θ is the angle between the two stubs.

The mutual inductance between the inner ring and the outer ring can be expressed as [55]:

$$M = \frac{1}{I_{or}}\int_{S_{ir}}\overline{B_{or}}\cdot(r_2 - r_1 - W_1)\overline{S_{ir}}(H) \qquad (11)$$

where I_{or} is a current on the outer ring, B_{or} is the magnetic flux density which is created by I_{or}, and S_{ir} is the area of the inner ring. During the relative rotation of the inner ring and the outer ring, mutual inductance between the two rings remains constant because the relative area of the inner and outer rings does not change.

The total inductance and total capacitance can be calculated as:

$$L_{tot} = \frac{L_1 L_2 - M^2}{L_1 + L_2 - 2M} \qquad (12)$$

$$C_{tot} = C_1 + C_2 + C_{gap} + C_{stub} + C_c \qquad (13)$$

The high-order resonant frequency of the dual ring antennas can be calculated as:

$$f_2 = \frac{1}{2\pi\sqrt{L_{tot}C_{tot}}} \qquad (14)$$

From the above formulas, it is not difficult to deduce that only the coupling capacitance between the stubs will vary with the relative rotation between the inner and outer rings, consequently causing the high-order resonant frequency shift. In practical applications, the rotation of the nut is connected to the relative rotation of the inner and outer rings if properly installed. Thus, the high-order resonant frequency of the sensor based on dual ring antennas can be taken as a characterization of the loosening state of the bolt. Finite element simulation in Ansoft HFSS further verifies the feasibility of the sensor as described in the next section.

3. Simulation

In this section, the monitoring performance of the proposed bolt

Table 1
Dimensions of the dual ring antennas with two stubs.

Parameters	r_1 (mm)	r_2 (mm)	W_1 (mm)	W_2 (mm)	g (mm)	h_2 (mm)
Dimensions	30	36	3	2	2	1.2

loosening sensor is simulated in ANSYS HFSS. The sensor consists of two ring antennas that can be utilized as radiation units for wireless interrogation, as well as two dielectric substrates, which can be used to secure the sensors to bolts and connection parts. In practical application, one ring antenna etched on a substrate is fixed on the nut, while the other ring antenna etched on a substrate is mounted on the connection parts. The two ring antennas each contain a stub that projects inward and outward, respectively, and the two stubs can serve as sensing units to transmit the angle of rotation for the nut caused by the bolt preload degradation.

3.1. Performance simulation

The finite element model of the sensor in ANSYS HFSS is shown in Fig. 6. Both ring patch antennas are made of copper, and the substrate of both are made of FR4 dielectric material. The two ring patch antennas are short-circuited together by two stubs which realize the current flow between the two ring antennas. This ensures the radiation performance of the antenna sensor. Further, the sensor is placed in a vacuum chamber, and the distance between the boundary of the vacuum chamber and the sensor is more than a quarter of the wavelength of the electromagnetic wave radiated by the antenna. This ensures the computational accuracy of the far-field radiation. The boundary conditions for the patch and the ground plane are both set to Perfect E, and the antenna is activated by a lumped port via a feed line.

In order to adapt to the size of bolts and obtain good performance, the dimension parameters of the dual-ring antenna sensor have been optimized, and the specific dimensional parameters have the same meaning as in Fig. 3 and as stated in Table 1.

Fig. 7 shows the current distribution of the optimized antenna at the fundamental and high-order resonant frequencies. The split of the outer ring prevents the continuous flow of current on the outer ring. Meanwhile, the stubs handle the current flow between the inner and outer
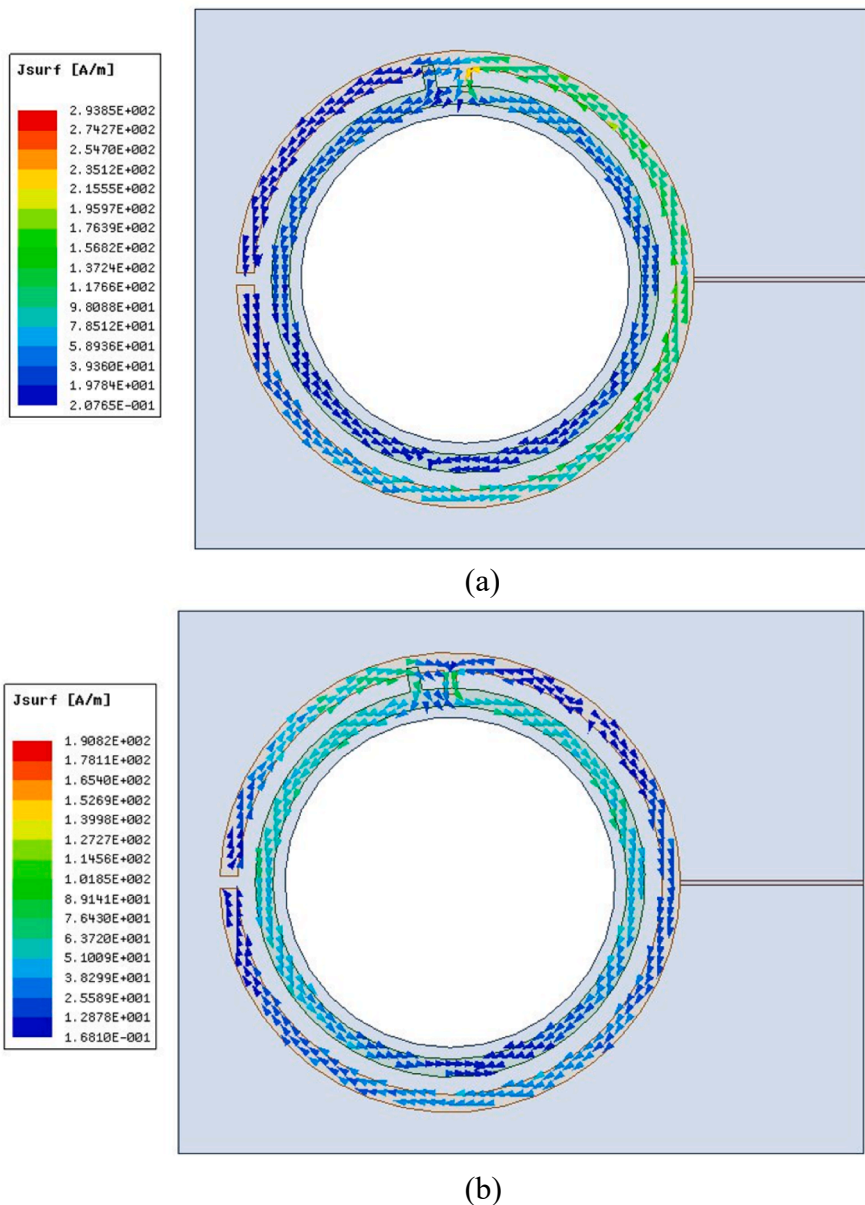
(a)

(b)

Fig. 7. Current distribution diagrams of dual ring antennas at (a) the fundamental resonant mode and at (b) the high-order resonant mode.

rings. It is obvious that the current distribution of the antenna is concentrated in the bottom right part of the outer ring at the fundamental resonant mode, and the rotation of the inner ring cannot change the capacitance of the fundamental resonant mode. Meanwhile, the current distribution of the antenna is concentrated in the top left part of the inner ring and in the outer ring at the high-order resonant mode. Thus, the rotation of the inner ring can change the value of the coupling capacitance between the two stubs, which causes a change in the total capacitance within the dual ring antennas at the high-order resonant mode.

According to the derivation of the theoretical formula, a change in the coupling capacitance will cause a shift in the resonant frequency. Thus, the antenna's resonance frequency can be used to characterize the status of the bolt. Then, the simulation of the working performance of the bolt loosening sensor is carried out in the ANSYS HFSS. The quality factor calculated by HFSS is 52.87. In the initial state, the two stubs overlap, and the inner ring rotates counterclockwise relative to the outer ring which simulates the rotation of the nut. Each rotation step of the inner ring is set at 2 degrees, and the reflection loss curve of the antenna

is depicted in Fig. 8. Fig. 9 shows the relation curve of the high-order resonance frequency and the rotation angle.

From the simulation results of the dual ring antennas, it is clear that the high-order resonant frequency of the antenna increases with the counterclockwise rotation of the inner ring, while the fundamental resonant frequency remains constant, which are constant with the theoretical derivation. The relationship between the high-order resonant frequency and rotation angle maintains good linearity within a specific range. The antenna's sensitivity is 2.40 MHz/degree, and the correlation coefficients of the fitted line in Fig. 9 is 0.9473. Thus, the status of the bolt's preload can be derived from the variations in the high-order resonant frequencies of the antenna.

3.2. Environment influence

In practical engineering applications, the performance of sensors will be affected by the surrounding environment, mainly temperature and humidity.

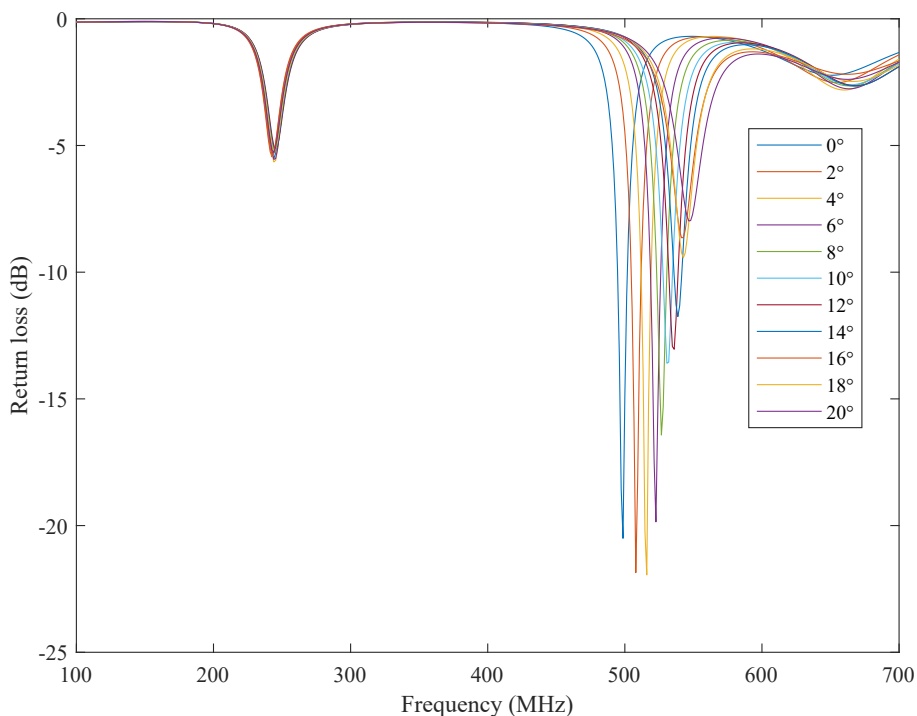Temperature can shift the resonant frequency of the sensor by

Fig. 8. The return loss curves of the antenna at different angles of rotation.
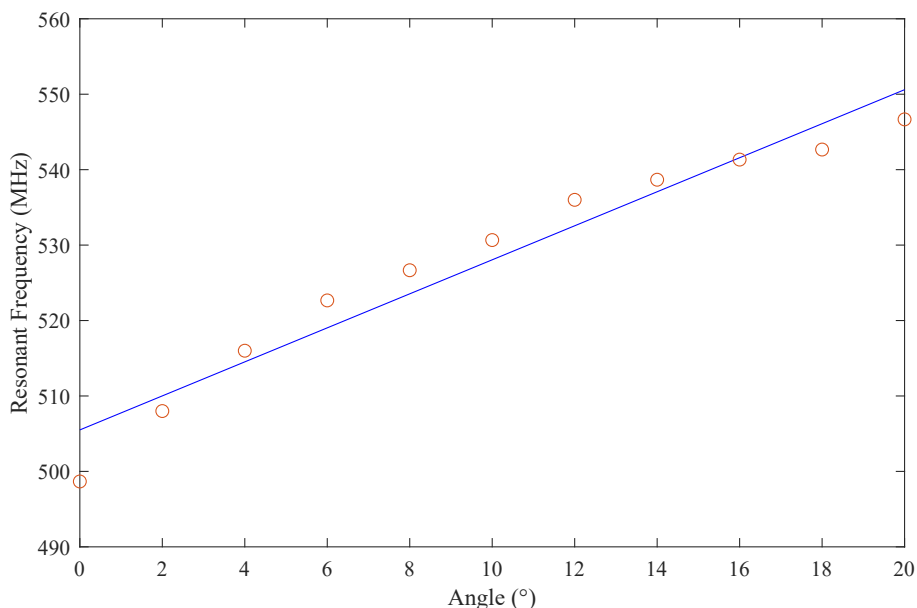

Fig. 9. Relationship between the angle of rotation and the antenna's high-order resonant frequency.

affecting the dielectric constant of the substrate and the size of the sensor. Related studies show that the change of dielectric constant is the main cause of the resonant frequency shift of the sensor [56]. Hence, only the temperature effect simulation of the dielectric constant of the substrate is performed in this section.

The substrate material of the proposed sensor is FR4, which has a relative dielectric constant of 4.4 at room temperature (20 °C). In addition, the thermal coefficient of dielectric constant (TCDk) of FR4 is 200 parts per million (ppm) per degree celsius (°C). The effect of temperature variations from −10 °C to 60 °C on sensor performance was simulated in HFSS, and the temperature step was set at 10 °C. Since the sensing variable of the sensor is the high-order resonant frequency and

the frequency offset caused by temperature is very small, only a small range of sweep is carried out at the high-order resonant frequency of the sensor to demonstrate the temperature effects in HFSS. The reflection loss curve of the antenna is depicted in Fig. 10. Fig. 11 shows the relation curve of the high-order resonance frequency and the temperature variations.

The simulation results show that the high-order resonant frequency decreases almost linearly with the increase of temperature, and the correlation coefficient is 0.9985. When the temperature increases by 10 °C, the high-order resonant frequency decreases by 0.11 MHz. And the sensor's sensitivity caused by nut's rotation is 2.40 MHz/degree. It is not difficult to find that the temperature change has little effect on the high-
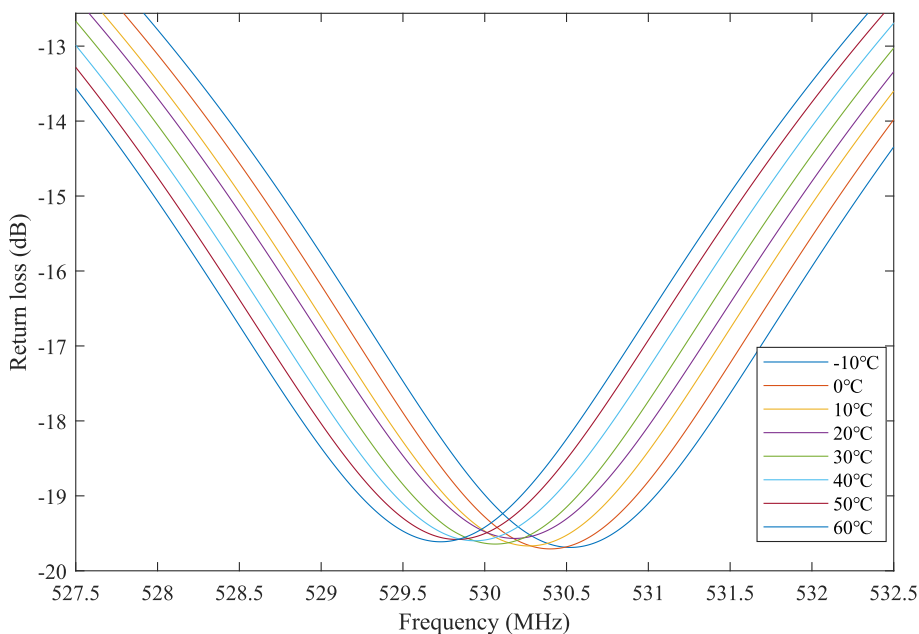
Fig. 10. The return loss curves of the antenna at different temperature.
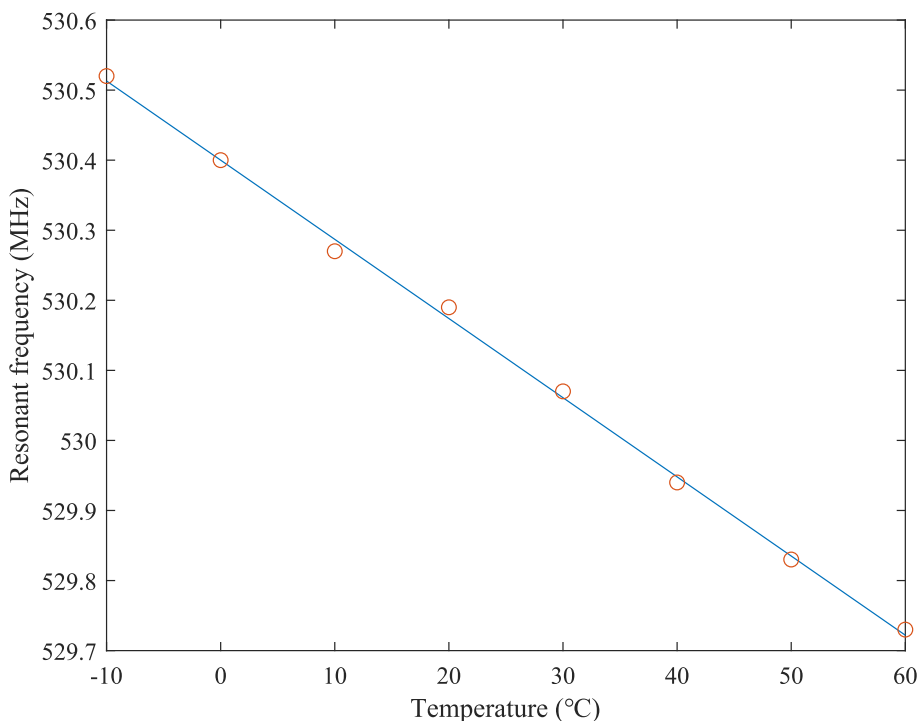

Fig. 11. Relationship between temperature and the antenna's high-order resonant frequency.

order resonant frequency of the sensor. In practical application, by establishing the relation between resonant frequency and temperature change, temperature compensation can be realized and the influence of temperature can be avoided.

Humidity has an important effect on the reflection coefficient of the antenna, but has little effect on the resonant frequency of the antenna [57]. The proposed sensor takes the high-order resonant frequency of the antenna as the sensing variable, and thus the influence of humidity on its performance can be ignored. Furthermore, the influence of humidity on antenna performance can be ignored when the moisture absorption rate of substrate material is less than 3% [58]. The moisture

absorption rate of FR4 is 0.2%, which means that the proposed sensor is immune to the effects of humidity.

In general, temperature effects can be avoided by temperature compensation, while humidity effects are smaller and can be ignored. Therefore, environmental influence was not taken into account in subsequent experiments.

4. Experiment

In order to validate and quantify the monitoring capabilities of the proposed sensor in bolt loosening, physical sensors were created and
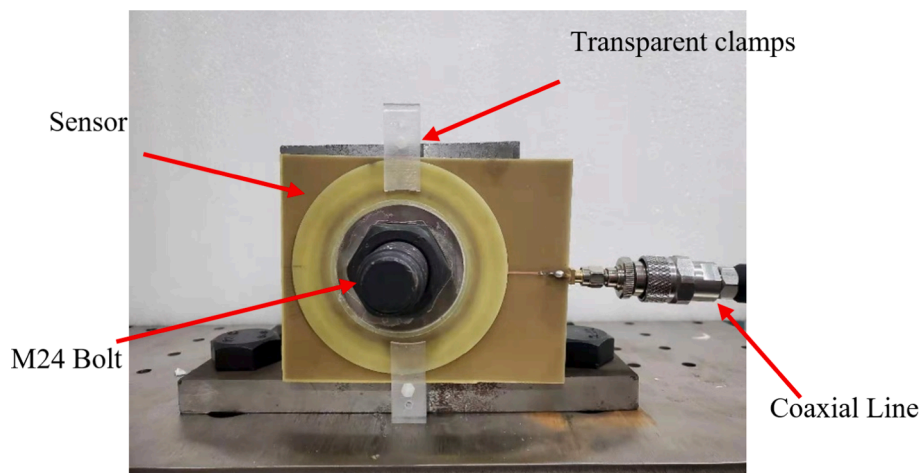
Fig. 12. The experimental setup.

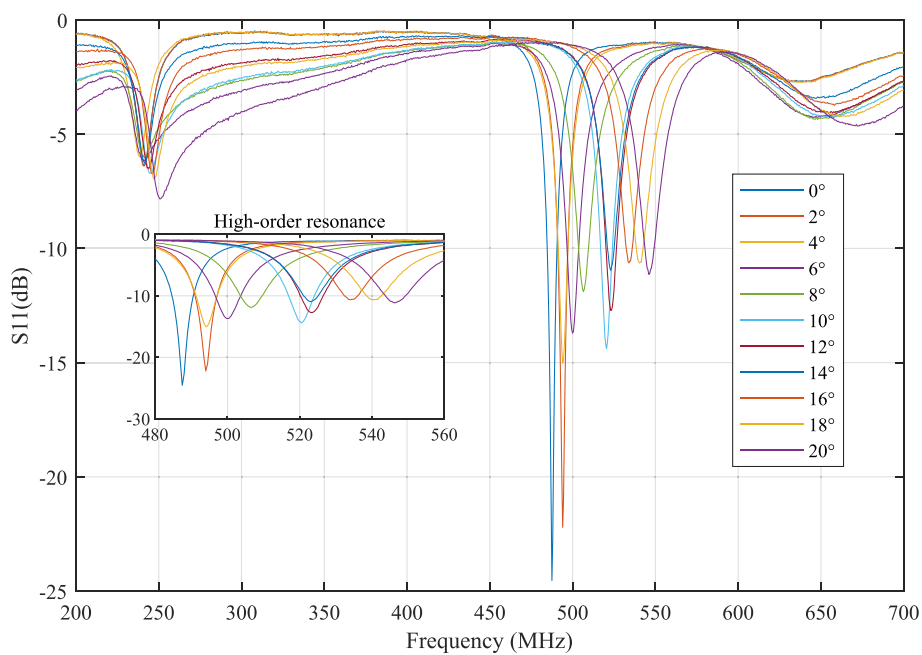**Fig. 13.** The dual ring antenna with two stubs for bolt loosening detection.

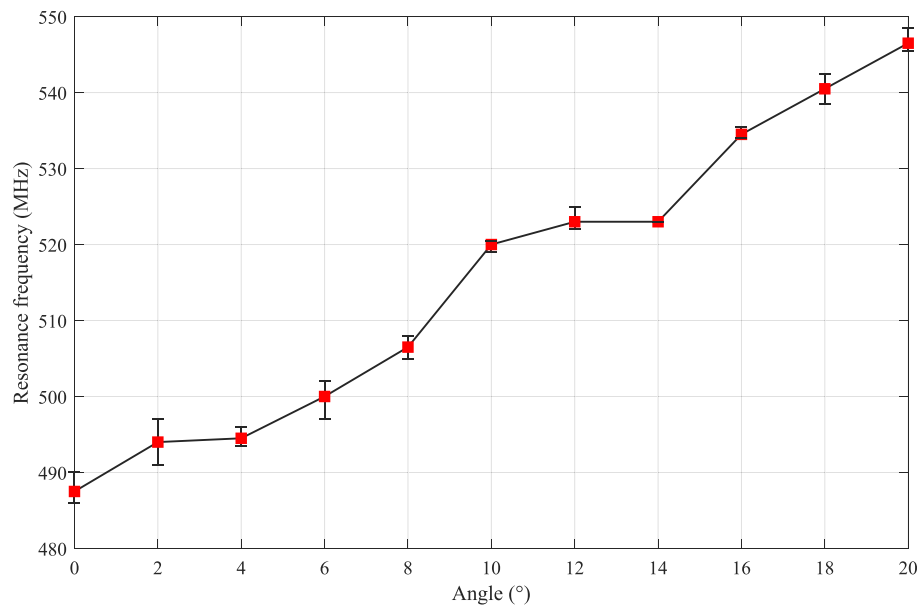**Fig. 14.** S11 curves of the antenna under different angles of rotation.

Fig. 15. Relationship between the angles of rotation and the resonant frequencies.

tested in the laboratory. The sensor used for this test consists of two sets of ring antennas, both made of copper, and the material used for the dielectric substrate is FR4-epoxy. Meanwhile, the size parameters of the physical sensor are consistent with the size parameters of the sensor in the simulation.

4.1. Instrumentation setup

The experimental setup is shown in Fig. 12. The sensor is attached to a bolt that secures the steel block platform in place, and the bolt chosen for this experiment was M24. The substrate of the outer ring antenna is fixedly connected with the rigid block by glue, which means the outer ring antenna will remain stationary while the bolt is loosening. While the inner ring antenna is connected with the nut through a transparent plate with a hexagonal hole in the center of the transparent plate, enabling the nut to be nested within the transparent plate, allowing the nut and inner ring antenna to rotate in lockstep.

The onsite installation of the sensor is shown in Fig. 13. The inner ring antenna and the outer ring antenna must be connected in the same plane; thus the inner ring antenna and the outer ring antenna are clamped together by transparent clamps. The dual ring antennas have a SMA connector at the end of the feedline, and a vector network analyzer (VNA) is connected to the SMA connector via a coaxial line, allowing the electromagnetic characteristics of the dual ring antennas to be retrieved.

Before the experiment started, the stubs of the inner and outer ring antennas were set to overlap, just like the initial state of the simulation. In order to accurately measure the loosening of the bolt, the relative rotation angle of the inner and outer ring antenna was marked with pencil on the outer ring antenna according to the protractor. Then the nut drove the inner ring antenna to rotate around the outer ring antenna, simulating the loosening of the bolt when the bolt's preload degrades. In the experiment, the nut rotation was set at 2° to quantitatively characterize the monitoring performance of the sensor. For accurate measurement, the nut stayed in place for 30 s after each rotation, and then the VNA recorded the S11 values of the sensor. In each bolt state, three groups of data were measured to obtain the corresponding return loss curve of the sensor. The resonant frequency of the sensor can be obtained by extracting the frequency at the local minimum of each return loss curve. The working performance of the sensor is discussed in the next section

Table 2
Simulation results and experiment results.

	Sensitivity (MHz/ degree)	Correlation coefficients (Linear fitting)	Starting high-order resonant frequency	Ending high-order resonant frequency
Simulation	2.40	0.9473	498.667	546.667
Experiment	2.95	0.9789	487.5	546.5

4.2. Experimental results and discussions

Fig. 14 shows the correlation curve between the S11 parameters and the frequencies of the dual ring antennas obtained from the test. Furthermore, the scatter diagram of the antenna's high-order resonant frequency and the various loosening states of the bolt are plotted in Fig. 15, and the error bar shows the range of frequencies.

According to the experimental results, it is obvious that the high-order resonant frequencies of the antenna drifts in an increasing direction with the decline of the bolt preload, while the fundamental resonant frequency of the antenna remains essentially unchanged during any bolt state, which is in good agreement with theoretical derivation and simulation. However, through observation of the experimental results, when the rotation angle of the nut is 2–4 degrees and 10–12 degrees, the high-order resonant frequency basically remains unchanged, which may be caused by the incomplete rotation of the inner ring inside the sensor during the experiment. From the whole experiment process, the high-order resonant frequency of the sensor shows an increasing trend with the loosening of the bolt, and the relationship between the high-order resonance frequency of the antenna and the rotation angle of the nut is linearly well fitted, implying that the state of the bolt's preload can be quantitatively analyzed by the high-order resonant frequency drift of the antenna.

Table 2 compares the results of the numerical simulation and the experiment. Sensitivity and correlation coefficients were obtained by the linear fitting of simulated and experimental results, respectively. Through comparison, it is not difficult to find that the simulation results are basically consistent with the experimental results, but there is a little discrepancy, which is mainly caused due to the following reasons:

1. In the HFSS simulation, the sensor was placed in an ideal vacuum environment, but there was electromagnetic interference, ambient temperature, and humidity interference in the laboratory, which caused

Table 3
Comparison with other types of sensors for bolt loosening monitoring.

Sensing Principle	Sensing variable	Sensor system	Installation requirements	Division value	Sensitivity	Sensor size	Refs.
Shielding of metal film	Reception of RF signal	Chipless UHF RFID (850–950 MHz)	No special needs	20 degree	–	135 mm × 80 mm	[44]
Change in electric length	Resonant frequency	Chipless UHF RFID (100 KHz-2.0 GHz)	The insulating layer coated around the bolt	12 degree	–	100 mm × 10 mm	[45]
Change in electric length	Resonant frequency	Chipless UHF RFID (2.9–3.0 GHz)	Hole in the bolt shaft	10 Nm	54.4 MHz/mm	47 mm × 45 mm	[43]
Capacitive coupling	Resonant frequency	Chipless UHF RFID (450–550 MHz)	No special needs	2 degree	2.95 MHz/degree	116 mm × 92 mm	This paper

the antenna's resonant frequency to fluctuate.

2. In the HFSS simulation, the sensor's inner ring antenna and outer ring antenna were located in the same plane, and the current flowed via the stubs. During the experiment, however, a thin layer of air remained between them, although the inner and outer ring antennas were clamped together by a transparent clamp.

3. There were some errors in the manufacturing process of the sensor. For instance, the welding of the feeding point introduced unwanted some effects.

Table 3 summarizes the performances of several different types of sensors for bolt loosening monitoring. By comparison, the sensitivity of the sensor proposed in this paper is relatively low; but the sensor can monitor the whole bolt loosening process, and the bolt does not need to be particularly constructed to suit the sensor installation criteria, which means that sensors can be adapted to in-service bolt monitoring.

5. Conclusions

This paper introduced a novel loosening detection method based on capacitive-coupled dual ring antennas, which can detect the whole process of bolt loosening and can be applied to in-service bolts. The sensor is made up of two concentric rings, operating at UHF frequency, one of which rotates synchronously with the nut and the other of which is fastened to the connected member, and the sensor's overall size is 116 mm × 92 mm × 2.4 mm. The rotation angle of the nut can indicate the loosening state of the bolt, which will affect the coupling capacitance inside the antenna, and then change the resonant frequency of the antenna. Equivalent-circuit models of the dual ring antennas are proposed to obtain the theoretical resonant frequency formula. Meanwhile, the finite element simulation in ANSYS HFSS were conducted to demonstrate the relationship between the antenna's resonant frequency shift and the bolt loosening. The antenna's quality factor calculated by HFSS is 52.87. Laboratory experiments was also carried out to verify the working performance of the sensor. The results of simulation and experiment both show that there is a good linear relationship between the resonance frequency and the rotation angle of the nut, and the correlation coefficients are 0.9473 and 0.9789 respectively. The sensitivities are 2.40 MHz/degree and 2.95 MHz/degree respectively. The difference is mainly due to environmental interference and fabrication errors. In the future, we will explore sensors in simpler configurations and the influence of ambient temperature and humidity on the proposed sensor to improve accuracy.

CRediT authorship contribution statement

Kang Jiang: Conceptualization, Methodology, Writing – original draft. **Liyu Xie:** Data curation, Writing – original draft, Writing – review & editing. **Songtao Xue:** Investigation, Writing – review & editing, Project administration. **Guochun Wan:** Software, Methodology, Writing – review & editing.

Declaration of Competing Interest

The authors declare the following financial interests/personal relationships which may be considered as potential competing interests: Liyu Xie has patent Bolt detection system based on double-opening resonant ring patch antenna licensed to Tongji University.

References

[1] L. Huo, F. Wang, H. Li, G. Song, A fractal contact theory based model for bolted connection looseness monitoring using piezoceramic transducers, Smart Mater. Struct. 26 (10) (2017) 104010.

[2] J. Xu, J. Dong, H. Li, C. Zhang, S.C. Ho, Looseness monitoring of bolted spherical joint connection using electro-mechanical impedance technique and BP neural networks, Sensors 19 (8) (2019) 1906.

[3] Y. Pan, Y. Ma, Y. Dong, Z. Gu, D. Wang, A Vision-Based Monitoring Method for the Looseness of High-Strength Bolt, IEEE Trans. Instrum. Meas. 70 (2021) 1–14.

[4] T. Wang, G. Song, S. Liu, Y. Li, H. Xiao, Review of bolted connection monitoring, Int. J. Distrib. Sens. Netw. 9 (12) (2013) 871213.

[5] F. Wang, G. Song, Bolt-looseness detection by a new percussion-based method using multifractal analysis and gradient boosting decision tree, Struct. Health Monitor. 19 (6) (2020) 2023–2032.

[6] Y. Jiang, M. Zhang, C.H. Lee, A study of early stage self-loosening of bolted joints, J. Mech. Des. 125 (3) (2003) 518–526.

[7] Q. Kong, J. Zhu, S.C.M. Ho, G. Song, Tapping and listening: A new approach to bolt looseness monitoring, Smart Mater. Struct. 27 (7) (2018) 07LT02.

[8] X. Zhao, Y. Zhang, N. Wang, Bolt loosening angle detection technology using deep learning, Struct. Control Health Monitor. 26 (1) (2019) e2292.

[9] C. Wang, N. Wang, S.-C. Ho, X. Chen, G. Song, Design of a new vision-based method for the bolts looseness detection in flange connections, IEEE Trans. Ind. Electron. 67 (2) (2020) 1366–1375.

[10] X. Quan, H. Lv, C. Liu, H. Wang, D. Wu, P. Chen, H. Zhou, An investigation on bolt stress ultrasonic measurement based on acoustic time difference algorithm with adaptive hybrid extended Kalman filter, Measurement 186 (2021) 110223.

[11] P. Razi, R.A. Esmaeel, F. Taheri, Improvement of a vibration-based damage detection approach for health monitoring of bolted flange joints in pipelines, Struct. Health Monitor. 12 (3) (2013) 207–224.

[12] M. Chen, B. Xu, Bolted joint looseness damage detection using electromechanical impedance measurements by PZT sensors, Third International Conference on Smart Materials and Nanotechnology in Engineering. International Society for Optics and Photonics, 2012, 8409: 840925.

[13] T.-C. Huynh, T.-D. Nguyen, D.-D. Ho, N.-L. Dang, J.-T. Kim, Sensor fault diagnosis for impedance monitoring using a piezoelectric-based smart interface technique, Sensors 20 (2) (2020) 510.

[14] S.K. Samantaray, S.K. Mittal, P. Mahapatra, S. Kumar, An impedance-based structural health monitoring approach for looseness identification in bolted joint structure, J. Civ. Struct. Health Monitor. 8 (5) (2018) 809–822.

[15] L. Huo, D. Chen, Q. Kong, H. Li, G. Song, Smart washer—A piezoceramic-based transducer to monitor looseness of bolted connection, Smart Mater. Struct. 26 (2) (2017) 025033.

[16] D. Chen, L. Huo, H. Li, G. Song, A fiber bragg grating (FBG)-enabled smart washer for bolt pre-load measurement: design, analysis, calibration, and experimental validation, Sensors 18 (8) (2018) 2586.

[17] S. Deshmukh, H. Huang, Wireless interrogation of passive antenna sensors, Meas. Sci. Technol. 21 (3) (2010) 035201.

[18] G. Marrocco, F. Amato, Self-sensing passive RFID: From theory to tag design and experimentation, 2009 European Microwave Conference (EuMC). IEEE, 2009: 001-004.

[19] J. Zhang, G. Tian, A. Marindra, A. Sunny, A.o. Zhao, A review of passive RFID tag antenna-based sensors and systems for structural health monitoring applications, Sensors 17 (2) (2017) 265.

[20] M. Alamin, G.Y. Tian, A. Andrews, P. Jackson, Corrosion detection using low-frequency RFID technology, Insight-Non-Destruct. Test. Condition Monitor. 54 (2) (2012) 72–75.

[21] R. Khalifeh, M. Segalen Yasri, B. Lescop, F. Gallee, E. Diler, D. Thierry, S. Rioual, Development of wireless and passive corrosion sensors for material degradation monitoring in coastal zones and immersed environment, IEEE J. Oceanic Eng. 41 (4) (2016) 776–782.

[22] S. Xue, Z. Yi, L. Xie, et al., A displacement sensor based on a normal mode helical antenna, Sensors 19 (17) (2019) 3767.

[23] S. Xue, K. Jiang, S. Guan, L. Xie, G. Wan, C. Wan, Long-Range Displacement Meters Based on Chipped Circular Patch Antenna, Sensors 20 (17) (2020) 4884.

[24] L.U. Daura, G.Y. Tian, Wireless power transfer based non-destructive evaluation of cracks in aluminum material, IEEE Sens. J. 19 (22) (2019) 10529–10536.

[25] A.M.J. Marindra, G.Y. Tian, Chipless RFID sensor for corrosion characterization based on frequency selective surface and feature fusion[J], Smart Mater. Struct. 29 (12) (2020) 125010.

[26] D. Girbau, A. Ramos, A. Lazaro, S. Rima, R. Villarino, Passive wireless temperature sensor based on time-coded UWB chipless RFID tags, IEEE Trans. Microw. Theory Tech. 60 (11) (2012) 3623–3632.

[27] J.J. Martínez-Martínez, F.J. Herraiz-Martínez, G. Galindo-Romera, Design and characterization of a passive temperature sensor based on a printed MIW delay line, IEEE Sens. J. 16 (22) (2016) 7884–7891.

[28] E.M. Amin, M.S. Bhuiyan, N.C. Karmakar, B. Winther-Jensen, Development of a low cost printable chipless RFID humidity sensor, IEEE Sens. J. 14 (1) (2014) 140–149.

[29] P. Fathi, S. Bhattacharya, N.C. Karmakar, Dual-polarized Keratin-based UWB Chipless RFID Relative Humidity Sensor, IEEE Sens. J. 22 (3) (2021) 1924–1932.

[30] C. Occhiuzzi, A. Rida, G. Marrocco, M. Tentzeris, RFID passive gas sensor integrating carbon nanotubes, IEEE Trans. Microw. Theory Tech. 59 (10) (2011) 2674–2684.

[31] R.A. Potyrailo, C. Surman, A passive radio-frequency identification (RFID) gas sensor with self-correction against fluctuations of ambient temperature, Sens. Actuators, B 185 (2013) 587–593.

[32] A.M.J. Marindra, G.Y. Tian, Multiresonance chipless RFID sensor tag for metal defect characterization using principal component analysis, IEEE Sens. J. 19 (18) (2019) 8037–8046.

[33] M. Borgese, F.A. Dicandia, F. Costa, S. Genovesi, G. Manara, An inkjet printed chipless RFID sensor for wireless humidity monitoring, IEEE Sens. J. 17 (15) (2017) 4699–4707.

[34] B. Wu, X. Zhang, B. Huang, Y. Zhao, C. Cheng, H. Chen, High-Performance wireless ammonia gas sensors based on reduced graphene oxide and Nano-Silver ink hybrid material loaded on a patch antenna, Sensors 17 (9) (2017) 2070.

[35] X. Xu, H. Huang, Battery-less wireless interrogation of microstrip patch antenna for strain sensing, Smart Mater. Struct. 21 (12) (2012) 125007.

[36] I. Mohammad, H. Huang, An antenna sensor for crack detection and monitoring, Adv. Struct. Eng. 14 (1) (2011) 47–53.

[37] J. Yao, F. Mbanya Tchafa, A. Jain, S. Tjuatja, H. Huang, Far-field interrogation of microstrip patch antenna for temperature sensing without electronics, IEEE Sens. J. 16 (19) (2016) 7053–7060.

[38] S. Xue, K. Xu, L. Xie, G. Wan, Crack sensor based on patch antenna fed by capacitive microstrip lines, Smart Mater. Struct. 28 (8) (2019) 085012.

[39] S. Caizzone, E. DiGiampaolo, Wireless passive RFID crack width sensor for structural health monitoring, IEEE Sens. J. 15 (12) (2015) 6767–6774.

[40] J. Zhang, B. Huang, G. Zhang, G. Tian, Wireless passive ultra high frequency RFID antenna sensor for surface crack monitoring and quantitative analysis, Sensors 18 (7) (2018) 2130.

[41] L. Xie, S. Xue, Z. Yi, et al., Double-frequency passive deformation sensor based on two-layer patch antenna, Smart Struct. Syst., Int. J. 27 (6) (2021) 969–982.

[42] Z. Yi, S. Xue, L. Xie, G. Wan, Detection of setting time in cement hydration using patch antenna sensor, Struct. Control Health Monit. 29 (1) (2022) e2855.

[43] S. Xue, X. Li, L. Xie, et al., A bolt loosening detection method based on patch antenna with overlapping sub-patch, Structural Health Monitoring, 2021: 14759217211055613.

[44] J. Wu, X. Cui, Y. Xu, A novel RFID-based sensing method for low-cost bolt loosening monitoring, Sensors 16 (2) (2016) 168.

[45] E. Matsunaga, M. Nakamura, T. Minotani, et al., Paintable wireless passive sensor based on electromagnetic waveguide to detect loose bolts for remote infrastructure inspection, 2019 IEEE Sensors. IEEE, 2019: 1-4.

[46] T.-C. Huynh, J.-H. Park, H.-J. Jung, J.-T. Kim, Quasi-autonomous bolt-loosening detection method using vision-based deep learning and image processing, Autom. Constr. 105 (2019) 102844.

[47] J.D. Baena, J. Bonache, F. Martin, R.M. Sillero, F. Falcone, T. Lopetegi, M.A. G. Laso, J. Garcia-Garcia, I. Gil, M.F. Portillo, M. Sorolla, Equivalent-circuit models for split-ring resonators and complementary split-ring resonators coupled to planar transmission lines, IEEE Trans. Microw. Theory Tech. 53 (4) (2005) 1451–1461.

[48] O. Sydoruk, E. Tatartschuk, E. Shamonina, L. Solymar, Analytical formulation for the resonant frequency of split rings, J. Appl. Phys. 105 (1) (2009) 014903.

[49] G. Irene, A. Rajesh, A dual-polarized UWB–MIMO antenna with IEEE 802.11 ac band-notched characteristics using split-ring resonator, J. Comput. Electron. 17 (3) (2018) 1090–1098.

[50] N. Pekçokgüler, G. Dündar, H. Torun, A.D. Yalçınkaya, A novel equivalent circuit model for split ring resonator with an application of low phase noise reference oscillator, Integration 61 (2018) 160–166.

[51] S. Naoui, L. Latrach, A. Gharsallah, Equivalent circuit model of double split ring resonators, Int. J. Microw. Opt. Technol. 11 (1) (2016) 1–6.

[52] J.A. Ansari, R.B. Ram, S.K. Dubey, P. Singh, A frequency agile stacked annular ring microstrip antenna using a Gunn diode, Smart Mater. Struct. 16 (6) (2007) 2040–2045.

[53] B.K. Kanaujia, B.R. Vishvakarma, Analysis of Gunn integrated annular ring microstrip antenna, IEEE Trans. Antennas Propag. 52 (1) (2004) 88–97.

[54] Bohua Gan, Liang Zhou, YaoPing Zhang, JunFa Mao, A dual-band microstrip antenna using a circular ring and a concentric disk, Int. J. RF Microwave Comput. Aided Eng. 26 (3) (2016) 268–276.

[55] S.H. Lim, Y.C. Oh, H. Lim, et al., Analysis and design of a UHF RFID tag antenna with a split ring resonator, 2008 International Workshop on Antenna Technology: Small Antennas and Novel Metamaterials. IEEE, 2008: 446-449.

[56] S. Xue, Z. Yi, L. Xie, G. Wan, Simulation and experiment on the temperature performance of sensors based on unstressed patch antennas, J. Harbin Eng. Univ. 42 (10) (2021) 1439–1445.

[57] S. Jain, P.K. Mishra, V.V. Thakare, J. Mishra, Microstrip moisture sensor based on microstrip patch antenna, Progr. Electromagn. Res. M 76 (2018) 177–185.

[58] C. Hertleer, A. Van Laere, H. Rogier, L. Van Langenhove, Influence of relative humidity on textile antenna performance, Text. Res. J. 80 (2) (2010) 177–183.